Temperature-dependent evaporation emission and gas/particle partitioning drive the seasonal dynamics of primary intermediate-volatility organic compounds

Hua Fang[1,2], Hongling Xu[2], Jun Li[3], Qina Jia[1], Shutan Ma[1], Xuanxuan Duan[1], Bing Hong[1], Ting Wu[1 *], Fuliu Xu[1], Xinming Wang[2*]

[1] School of Ecology and Environment, Anhui Normal University, Wuhu, 241002, China

[2] State Key Laboratory of Advanced Environmental Technology, Guangzhou Institute of Geochemistry, Chinese Academy of Sciences, Guangzhou, 510640, China

[3] Wuhu Ecological and Environmental Monitoring Center of Anhui Province, Wuhu, 241005, China

*Corresponding authors:

Dr. Ting Wu (wuting19@mail.ahnu.edu.cn)

Dr. Xinming Wang (wangxm@gig.ac.cn)

Abstract

Intermediate-volatility organic compounds (IVOCs) serve as crucial precursors to secondary organic aerosol (SOA), yet their seasonal variations remain insufficiently characterized, impeding a comprehensive understanding of their atmospheric processing and impacts on air quality. To capture the seasonal dynamics of primary IVOCs and identify the key drivers governing their variability, four-season field campaigns were conducted at an urban site in Yangtze River Delta region. The total concentration of measured IVOCs was 1228.2 ± 132.7 ng m^{-3} (average ± 95% confidence interval), dominated by long-chain alkanes. A distinctive summer-maximum and winter-minimum pattern was identified for measured IVOCs, contrasting sharply with typical seasonal trends of most primarily-emitted air pollutants. This pattern was driven by enhanced temperature-dependent evaporative emissions and efficient particle-to-gas partitioning of low-volatility IVOCs during warm seasons. Petroleum-related sources were confirmed as the dominant contributors to the measured IVOCs. Positive matrix factorization (PMF) model further revealed evaporative emissions as the largest contributor (38.9%), followed by vehicle exhaust (37.7%), gas/particle partitioning (14.8%), and industrial emissions (8.6%). Our findings elucidate the critical roles of temperature-dependent emissions and gas/particle partitioning in shaping the seasonal cycle of IVOCs, and highlight the potentially expanding contribution of evaporative sources to urban IVOC loads under future climate change scenarios.

1. Introduction

Intermediate-volatility organic compounds (IVOCs) are defined as organic compounds with effective saturation concentrations (C*) ranging from 300 to 3×10^6 μg m^{-3}, roughly corresponding to the volatility of C_{12}–C_{22} normal alkanes (n-alkanes) (Donahue et al., 2012; Zhao et al., 2024a). As potent precursors to secondary organic aerosol (SOA), IVOCs exhibit high SOA mass yields upon atmospheric oxidation, thereby profoundly affecting air quality, regional climate, and human health (Robinson et al., 2007; McDonald et al., 2018). Cumulative evidence from bottom-up emission inventories and top-down observational studies has consistently demonstrated that IVOC-driven SOA production surpasses that from traditional SOA precursors, volatile organic compounds (VOCs), by 1–2 orders of magnitude (Fang et al., 2022; Manavi et al., 2022). During episodes of particulate pollution, IVOCs can contribute 35%−80% of the total SOA mass (Yang et al., 2019; Li et al., 2021; Wu et al., 2021a). Despite their pivotal role in SOA formation and atmospheric chemistry, research on IVOCs, particularly in complex real-world atmospheric matrices, remains notably insufficient compared to that on traditional VOCs (Ling et al., 2022).

Early efforts to quantify IVOC contributions to SOA formation have heavily relied on atmospheric models. However, the paucity of robust observational constraints has plagued these modeling frameworks. Most modeling studies derive IVOC emissions from scaling factor applied to VOC or primary organic aerosol (POA), yet the applicability of these factors is compromised by the spatiotemporal heterogeneity of emission sources and their strong dependence on emission type. This inherent variability inevitably propagates considerable uncertainty into SOA predictions (Pennington et al., 2021; Yang et al., 2024). Driven by the need for more accurate data inputs to models, recent studies have strived to directly characterize IVOC emissions from major anthropogenic sources, including vehicle exhaust (Drozd et al., 2019; Fang et al., 2021a), ship emissions (Huang et al., 2018; Liu et al., 2022), gasoline evaporation (Wang et al., 2025), and residential solid fuel combustion (Qian et al., 2021). Undoubtedly, these measurement-based studies have provided crucial emission profiles of IVOCs and established real-world relationships between IVOCs and co-emitted pollutants, laying a foundation for model refinement and field-based source apportionment of IVOCs (Fang et al., 2022; Yang et al., 2024; Scholz et al., 2025; Wu et al., 2025b).

Nevertheless, investigations on ambient IVOCs remain scarce compared to emission source studies (Tang et al., 2023). While a handful of field observations have reported IVOC concentrations, chemical compositions, and estimated SOA formation potentials, sources and influential factors contributing to ambient IVOC variations were inadequately resolved and quantified (Zhao et al., 2014; Tanzer-Gruener et al., 2022; Wernis et al., 2022). More importantly, most existing observations have relied on short-term sampling limited to one or two seasons, leaving a critical gap in understanding the systematic seasonal patterns of

ambient IVOCs (Tong et al., 2024; Hou et al., 2026). Modeling studies have already corroborated the seasonality of IVOC-derived SOA contributions. For instance, Yang et al. (2014) documented the highest fractional SOA contribution from IVOCs in winter (66.4%−80.7%), followed by spring (45.4%−65.8%), fall (41.3%−60.4%), and summer (35.8%−53.2%). In addition, seasonal temperature fluctuations could influence the gas/particle partitioning of low-volatility IVOCs (Fang et al., 2022), leading to the changes in their atmospheric abundance, phase distribution, and subsequent SOA formation. Consequently, a thorough investigation of the seasonal characteristics of ambient IVOCs is critical for elucidating their atmospheric processing and eventual contributions to SOA formation.

Herein, field campaigns covering four seasons were carried out at an urban site in the Yangtze River Delta region (YRD). We targeted 16 representative IVOC species, including 11 n-alkanes (nC_{12} − nC_{22}), 2 branched alkanes, and 3 polycyclic aromatic hydrocarbons (PAHs). These species are well-recognized as key IVOC surrogates, with established utility for constraining IVOC emissions, facilitating source apportionment, and estimating SOA formation potential (Pye et al., 2010; Hodzic et al., 2016; Fang et al., 2021b; Tang et al., 2021; Galeazzo et al., 2024). By quantifying these species and analyzing their seasonal patterns, this study advances the understanding of IVOC behaviors in complex urban atmospheres. Our findings not only provide valuable implications for refining regional air quality modeling frameworks, but also underpin the formulation of seasonally tailored IVOC control strategies for urban areas.

2. Methodology

2.1 Field experiments

As illustrated in Figure S1, sampling was carried out at an urban site within the YRD, China, during 2024. Field campaigns covered four seasons: spring (April 21−27), summer (July 4−10), fall (October 9−15), and winter (December 14−20). Each seasonal campaign lasted approximately one week, which may not capture the full spectrum of seasonal meteorological variability. Nonetheless, the variation trends of meteorological parameters (e.g., temperature) and air quality parameters ($PM_{2.5}$, CO, SO_2, NO_2, and O_3) recorded during each campaign broadly agreed with the corresponding seasonal features of this region (Table S2). The seasonal patterns reported herein should thus be interpreted as representative of typical seasonal conditions. The sampling location was a rooftop approximately 20 m above ground level, representative of a typical urban setting under the influence of mixed vehicular, commercial, and residential emission sources. This site was situated 100 m from a government-operated air quality monitoring station. For IVOC collection, an automated 12-channel sampler (JEC921, Jectec Science and Technology Co., Ltd., Beijing, China) equipped with Tenax TA/Carbograph 5TD sorbent tubes (Markes International, UK) was

deployed. We placed a PTFE filter (47 mm diameter, Whatman, UK) upstream of the sorbent tubes to exclude particulate matter. The sampler operated at a constant flow of 600 mL min^{-1}, with daily collections scheduled in eight 2-hour windows from 04:00 to 20:00 local time. To account for potential contamination during field observation, two blank tubes were collected each season, processed identically to ambient samples except that the pump remained off. The IVOCs in field blanks were either not detected or below the method detection limits (MDLs), indicating negligible background contamination. In total, 224 valid samples (including 8 field blanks) were obtained for subsequent laboratory analysis. Meteorological variables and other air pollutants ($PM_{2.5}$, CO, SO_2, NO_2, and O_3) were from the monitoring station. Concurrently, VOC measurements were performed using an online GC-MSD/FID system (TH300B, Wuhan Tianhong Instrument Co., Ltd., China). Further details on the VOC analysis are provided in Text S1.

2.2 Laboratory analysis

IVOC samples were analyzed using a thermal desorption system (TD-100, Markes International, UK) coupled to an Agilent 8890 gas chromatograph (GC) and a 5977C mass selective detector (MSD) (Agilent Technologies, Inc., CA, USA). First, each tube was heated to 320 °C for 15 min under high-purity helium (99.999%) to release the trapped analytes. Then the target compounds were cryo-focused on a cold trap maintained at −10 °C, followed by rapid thermal injection into the GC/MSD for chromatographic separation and mass spectrometric detection. Separation was achieved on an HP−5MS capillary column (30 m × 0.25 mm × 0.25 μm, Agilent Technologies, Inc., CA, USA). The column oven was temperature-programmed as follows: initial hold at 50 °C for 5 min, ramp to 280 °C at 5 °C min^{-1}, and final hold for 20 min. The MSD was operated in SCAN mode with electron impact ionization at 70 eV. Target IVOCs were identified by comparing their GC retention times and mass fragmentation patterns with those of authentic standards, and their concentrations were determined via external calibration.

2.3 Quality assurance/Quality control (QA/QC)

Prior to deployment, we conditioned all sorption tubes at 320 °C under a helium stream (100 mL min^{-1}, 99.999% purity). Each cleaned tube was subsequently analyzed by TD-GC/MSD to confirm the absence of residual IVOC contamination. Only tubes showing no detectable target species or concentrations below the established MDLs were approved for field use. The MDLs for the IVOC species quantified in this work was 0.57–4.72 ng m^{-3}. Upon sampling, the tube samples were promptly placed into a cool box (4 °C), transported to the laboratory, and stored at −18 °C until analysis. All samples were analyzed within one week. We evaluated potential sampling breakthrough by connecting two sorbent tubes in tandem during ambient air collection and analyzing both tubes afterward. The rear-tube IVOC loading was below 3% of that in the front tube, confirming that breakthrough was negligible

throughout the sampling periods. In addition, thermal desorption efficiency was assessed by subjecting selected sampled tubes to two successive thermal desorption cycles and computing the fraction of IVOCs quantified in the first cycle relative to the combined amount from both cycles. The average desorption efficiency was determined to be 98.6% ± 1.2% in this study.

2.4 Positive matrix factorization (PMF) model

To identify and quantify the main contributor to observed IVOCs, we applied U.S. Environmental Protection Agency (US-EPA) PMF 5.0 software to the dataset. Since PMF methodology has been detailed in earlier studies (Wang et al., 2016), only essential operational settings are summarized in the present work. A total of 19 species (13 alkanes, 3 PAHs, CO, SO_2, and NO_2) were incorporated into the input matrix, with all concentration values exceeding their respective MDLs. For each data point, we computed the associated uncertainty using the formulation of $Unc = [(EF \times c)^2 + (0.5 \times MDL)^2]^{1/2}$, where EF and c denote the error fraction and the species concentration, respectively. Multiple model runs were conducted with factor numbers ranging from 3 to 8. Criteria including solution stability, consistency between modelled and observed IVOC concentrations, and the rationality of factor profiles were used to evaluate different solutions. On this basis, the 4-factor solution was judged to be the most physically meaningful. Additional procedural details are provided in Text S2.

2.5 Statistical analysis

All statistical analysis was performed using SPSS software. Since Kolmogorov-Smirnov test showed that IVOC data were not normally distributed, seasonal differences in IVOC concentrations were evaluated using the nonparametric Kruskal-Wallis test. Relationships between IVOCs and other variables were examined with Spearman's correlation. Statistical significance was determined at $p < 0.05$.

3. Results and discussion

3.1 Ambient levels and volatility distributions of measured IVOCs

From Table S3, the total concentration of IVOCs measured during the sampling periods was 1228.2 ± 132.7 ng m^{-3} (average ± 95% C.I.). As speciated IVOCs, this level substantially exceeded those reported in Pasadena, USA (2.0 − 81.0 ng m^{-3}) (Tanzer-Gruener et al., 2022), was comparable to that measured in megacity Guangzhou in fall (1532.2 ± 189.0 ng m^{-3}) (Fang et al., 2022), but significantly lower than wintertime observations in megacity Shanghai (~ 5265.0 ng m^{-3}) (Li et al., 2019). Long-chain alkanes constituted the dominant component of measured IVOCs throughout the campaign, accounting for over 85% of the total mass. It was noteworthy that gaseous long-chain alkanes (> C_{12}) have always been missed in previous field observations (Li et al., 2022). In fact, these compounds, particularly those falling within the volatility range of nC_{12} − nC_{22}, predominantly existed in gas phase under ambient conditions (Fang et al., 2020; Tang et al., 2022). Although some earlier studies detected

particle-bound $nC_{12} - nC_{22}$ using quartz filter sampling, such measurements may have been influenced by positive sampling artifacts (e.g., adsorption of gaseous species onto filters) (Presto et al., 2012). Table S4 shows that the gaseous long-chain alkane concentrations measured here exceeded previously reported particle-phase values by 1−2 orders of magnitude. In terms of absolute levels, our observations were substantially higher than those in London, yet fell within the range reported for Chinese megacities like Beijing and Guangzhou. The measured gas-phase PAHs summed to 141.3 ± 12.3 ng m^{-3}, with naphthalene (Nap) being the most abundant species, sharing 73.9% ± 1.3% of the total PAHs. This aligns with earlier studies identifying Nap as the predominant species among gaseous PAHs (Huang et al., 2019; Tang et al., 2020; Fang et al., 2021b; An et al., 2024; Hou et al., 2026). As shown in Table S3, the Nap concentration measured in this study was lower than that in the northern Beijing–Tianjin–Hebei region (0.73 ± 0.31 μg m^{-3}) (Tang et al., 2020), fell within the range reported for Shanghai (38.0 − 2400.0 ng m^{-3}) (Li et al., 2019; An et al., 2024), and was higher than that in Guangzhou (94.0 ± 23.1 ng m^{-3}) (Fang et al., 2021b).

Figure 1 shows the volatility distribution of measured IVOCs throughout the entire observation period. In line with previous studies, IVOCs were dominated by high-volatility species. Specifically, compounds with the $\log_{10}C^*$ of 6, 5, and 4, corresponding to the volatility ranges of $nC_{12} – nC_{13}$, $nC_{14} – nC_{15}$, and $nC_{16} – nC_{17}$, respectively, accounted for 35.6 ± 2.3%, 28.3 ± 1.0%, and 22.5 ± 1.3% of the total IVOC mass. As shown in Figure S2, the stronger correlations among IVOCs of comparable volatility indicated that they shared similar sources and atmospheric processes. The volatility distribution of measured IVOCs, on the one hand, was subject to the influence of primary emission sources. IVOCs emitted from typical anthropogenic sources follow a volatility gradient: gasoline exhaust > diesel exhaust > heavy oil exhaust, which aligns with the volatility sequence of the corresponding unburned fuels (Fang et al., 2022; Liu et al., 2022). Gasoline exhaust is dominated by species with $\log_{10}C^* = 6$ (Zhao et al., 2016), whereas diesel exhaust contains a higher proportion of compounds with $\log_{10}C^* = 5$ and 4 (Zhao et al., 2015). In contrast, heavy oil combustion emissions exhibit relatively more low-volatility IVOCs ($\log_{10}C^* \leq 3$) (Huang et al., 2018). Moreover, previous studies have also reported that exhaust-IVOC volatility distribution was significantly governed by the properties of unburned fuels (Zhao et al., 2015; Tang et al., 2021). IVOCs in combustion exhaust generally exhibit higher volatility than their parent fuels, which could be the reason that combustion process fragments the long-chain carbons and shifts the volatility distribution of IVOCs toward higher values (Cui et al., 2022). On the other hand, atmospheric processes can further modify the volatility distribution of IVOCs following their emission into the ambient air. For instance, Fang et al. (2022) demonstrated that gas/particle partitioning exerted a pronounced influence on low-volatility IVOCs, with approximately 20% of these compounds repartitioning into the particle phase during their observational

campaigns. This dynamic repartitioning process thus reduced the abundance of low-volatility IVOCs in the gas phase. Collectively, the observed volatility distribution of IVOCs was governed by three key factors: the intrinsic chemical composition of parent fuels, source-dependent IVOC formation pathways (e.g., combustion-derived exhaust emissions or direct volatilization from unburned fuels), and subsequent atmospheric processing.

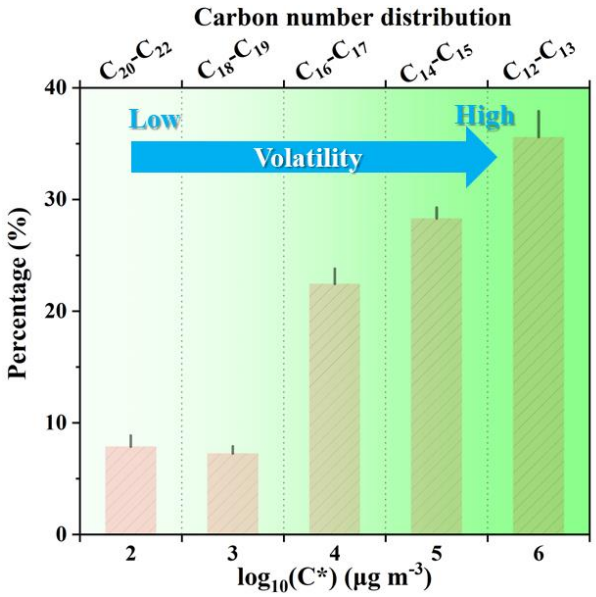


Figure 1. Volatility distributions of measured IVOCs based on the effective saturation concentration (C*, μg m^{-3}) and carbon numbers of normal alkanes. The error bar represents 95% confidence interval.

3.2 Seasonal variations

As shown in Figure 2, the concentration of IVOCs was significantly higher in summer than in the other three seasons ($p < 0.05$). No statistical difference in IVOC concentrations was observed between spring and fall. Unexpectedly, IVOCs reached its minimum in winter. This was contrary to the common winter-maximum pattern reported for primarily-emitted air pollutants. Table S3 illustrates such a pattern for SO_2, CO, NO_2, and $PM_{2.5}$, all of which demonstrated markedly elevated levels during winter relative to summer. Previous studies have reported that total IVOC concentrations during winter haze events were roughly double those observed in summer (Li et al., 2019; Tang et al., 2023). This elevated concentration in winter was mainly due to suppressed photochemical degradation and unfavorable meteorological conditions that limited pollutant dispersion. The seasonal pattern of measured IVOCs in this study was opposite to that reported in the Shanghai (Li et al., 2019), despite both sites being located within the YRD region. This could be attributed to differences in the range of measured species. Only gas-phase IVOCs were measured here, whereas both gas- and particle-phase IVOCs were collected during Shanghai observation. Furthermore, Li et al. (2019) conducted their IVOC sampling during winter haze episodes, where atmospheric

pollution levels and meteorological conditions differed substantially from those encountered in our study. This could further amplify the observed variations of IVOCs between the two studies. As shown in Table S3, higher atmospheric boundary layer height (BLH) in summer facilitated dispersion of IVOCs detected in this study, while summer peak in Ox (NO_2 + O_3) levels further accelerated photochemical consumption of these compounds. Both processes would theoretically act to lower IVOC concentrations in summer. Consequently, the unexpected summer-maximum IVOC concentration pattern observed in this study, wherein target IVOCs consist of primary hydrocarbons, was most plausibly ascribed to enhanced emissions of temperature-sensitive sources. Furthermore, the total concentration of measured IVOCs exhibited a significant correlation with ambient temperature (r=0.44, p<0.01), providing direct observational evidence for the temperature-driven enhancement of IVOCs. Similarly, Ait-Helal et al. (2014) reported elevated concentrations of gaseous nC_{12}–nC_{16} IVOCs in Paris during summer relative to winter, attributing this distinct seasonal pattern to variability in emission source strength and activity. As shown in Figure S3, IVOCs exhibited distinct diurnal profiles across both volatility fractions and seasons. In general, primarily-emitted air pollutants typically displayed a daytime minimum and nighttime maximum, a pattern driven by intensified photochemical degradation and elevated BLH during daylight hours. High-volatility IVOCs (nC_{12}–nC_{13}) conformed to this canonical diurnal trend across all four seasons (Figure S3). With decreasing volatility, however, IVOC diurnal patterns grew increasingly complex. For example, nC_{16}–nC_{17} compounds showed elevated daytime concentrations in spring. The daytime-minimum and nighttime-maximum pattern was particularly pronounced in summer for most IVOC species, with the exception of low-volatility nC_{20}–nC_{22}. The divergent diurnal patterns observed across volatility fractions implied that ambient IVOC concentrations were controlled by a suite of volatility-dependent regulatory mechanisms.

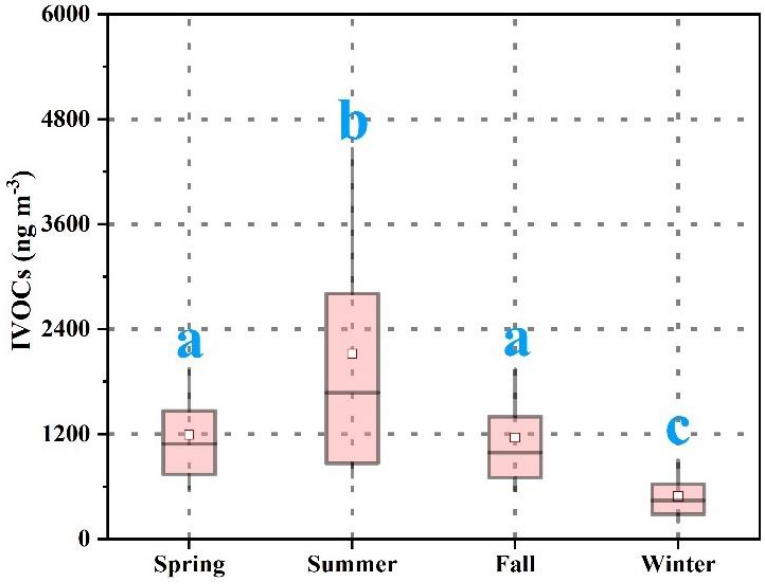


Figure 2. The total IVOC concentrations measured in different seasons. The squares and the central line represent the average and median values, respectively. The boxes represent the 25th and 75th percentiles, and the whiskers represent the 10th and 90th percentiles. Different letters denote statistically significant differences at $p < 0.05$ among four seasons.

From Table S3, high-volatility IVOCs ($\log_{10}C^* = 6$) were present at lower concentrations in summer relative to spring and fall. Conversely, the two methylnaphthalenes (MNs) attained seasonal maxima in summer. As displayed in Figure 3, the concentrations of nC_{14}–nC_{18} IVOCs measured in summer were significantly higher than those in the other three seasons, with this fraction dominating summer maximum in total IVOC concentration. Low-volatility IVOCs (nC_{19}–nC_{22}) exhibited the greatest abundances in summer. Of note, these low-volatility species were nearly undetectable during the cold winter (Figure 3), which was at least partially due to their preferential partitioning into the particle phase under low ambient temperature (4.9 ± 1.0 °C, Table S3). This observation was consistent with higher gas/particle partitioning coefficients (Kp) for these species at lower temperature (Fang et al., 2022).

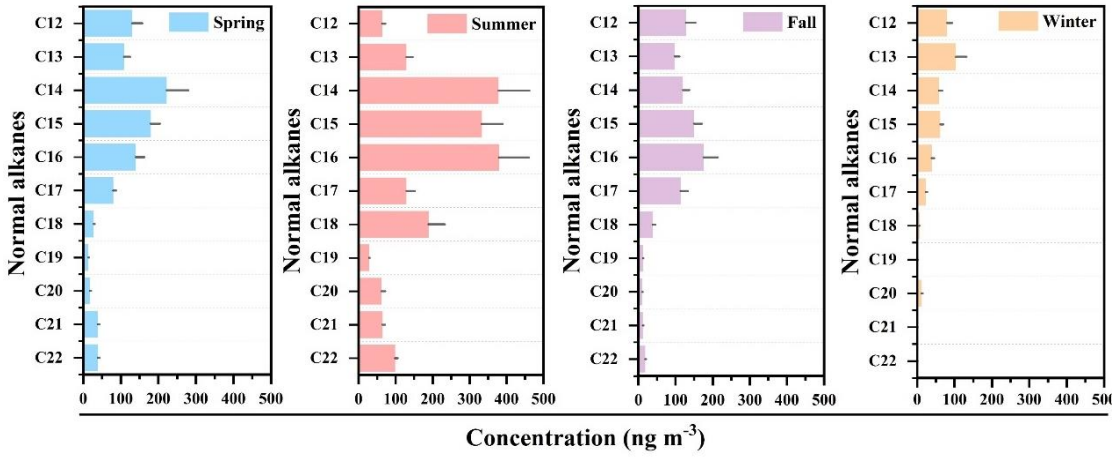


Figure 3. Concentrations of C_{12}-C_{22} normal alkanes measured in different seasons. Error bar is 95% confidence interval.

As illustrated in Figure 4, IVOCs exhibited a clear volatility-dependent response to increasing $PM_{2.5}$ concentrations. Moderate- and low-volatility IVOCs (e.g., nC_{14}–nC_{22}) underwent a pronounced exponential decay with rising $PM_{2.5}$ concentrations, and this trend intensified progressively as IVOC volatility decreased. However, concentrations of high-volatility IVOCs (nC_{12}–nC_{13}) showed no statistically significant correlation with $PM_{2.5}$. This exponential decline of nC_{14}–nC_{22} from the gas phase was largely consistent with their low saturation vapor pressures, which yield high Kp, and suggested that gas/particle partitioning was a dominant, though not exclusive, control on their gaseous abundances (Gou et al., 2021;

Lumiaro et al., 2021). As $PM_{2.5}$ concentrations increased, the partitioning equilibrium shifted decisively toward the condensed phase, driving a nonlinear decline in the gaseous abundances of these species. The enhanced sensitivity to $PM_{2.5}$ observed from nC_{14}–nC_{15} to nC_{20}–nC_{22} aligned closely with their decreasing volatility and corresponding increases in K_p values. Conversely, the insensitivity of high-volatility nC_{12}–nC_{13} to $PM_{2.5}$ variations was consistent with their high saturation vapor pressures and low K_p values, such that their gaseous concentrations remained largely unaffected by aerosol loading (Figure 4). Notably, $PM_{2.5}$ concentration could covary with ambient temperature, BLH and primary emission intensity on seasonal timescales, any of which may partly contribute to the observed decline in gaseous low-volatility IVOCs. Sensitivity to $PM_{2.5}$ strengthened monotonically with decreasing volatility (nC_{14}–nC_{15} to nC_{20}–nC_{22}), consistent with the expected increase in Kp. In contrast, high-volatility nC_{12}–nC_{13} remained insensitive to $PM_{2.5}$ loading, even though they were subject to identical emission and meteorological drivers. This species-selective, Kp-dependent pattern, alongside with the independent gas/particle partitioning factor resolved via PMF, cannot be attributed merely to generic covariation. Nevertheless, particle-bound IVOCs were not measured here. Next work is therefore recommended to conduct concurrent measurements of both gas- and particle-phase IVOCs to further elucidate the linkage between $PM_{2.5}$ and low-volatility IVOCs. Overall, this volatility-ordered, Kp-tracking dependence on $PM_{2.5}$ concentration serves as a fingerprint of partitioning rather than an emission-driven signal. The latter is controlled by source activity and temperature, not by $PM_{2.5}$ concentrations.

During the campaign, the IVOC concentrations, except for the high-volatility nC_{12} − nC_{13}, increased exponentially with ambient temperature and the strength of this exponential dependence increased as compound volatility decreased (Figure 4). Previous laboratory evaporative experiments reported exponential increases in IVOC concentrations with rising temperature (Wang et al., 2025). Thus, our findings suggested that evaporative emissions could represent an important contributor to observed IVOCs, with enhanced emission strength under warmer conditions driving summer maximum in IVOC concentrations. As a typical gaseous tracer for evaporative emissions (Zhang et al., 2013), isopentane is not subject to gas/particle partitioning and exhibits pronounced summertime enhancement (Figure S4), indicative of temperature-dependent evaporative emission processes. In addition to direct evaporative emissions, warming conditions further elevated gaseous IVOC concentrations by promoting the volatilization of low-volatility species from particles into the gas phase (Chen et al., 2025; Kong et al., 2025). IVOC–temperature relationship exhibited substantial complexity across different temperature regimes. For instance, below 15 °C, nC_{20} – nC_{22} showed no significant temperature dependence, whereas nC_{14} – nC_{15} and nC_{16} – nC_{17} displayed positive correlations with temperature. In contrast, nC_{12} – nC_{13} exhibited a negative correlation within three temperature intervals (<15 °C, 15–30 °C, >30 °C), and the negative

trend intensified at higher temperatures (Figure S6), primarily due to more vigorous photochemical degradation. Within 15°C – 30 °C range, only nC_{20} – nC_{22} maintained a robust positive correlation with temperature, while all other IVOC fractions exhibited negative correlations (Figure S6). The variable IVOC–temperature relationships observed across different temperature regimes arose from the combined and competing effects of temperature-dependent emissions (e.g., evaporative emission) and concurrent atmospheric processing (e.g., gas/particle partitioning and photochemical consumption).

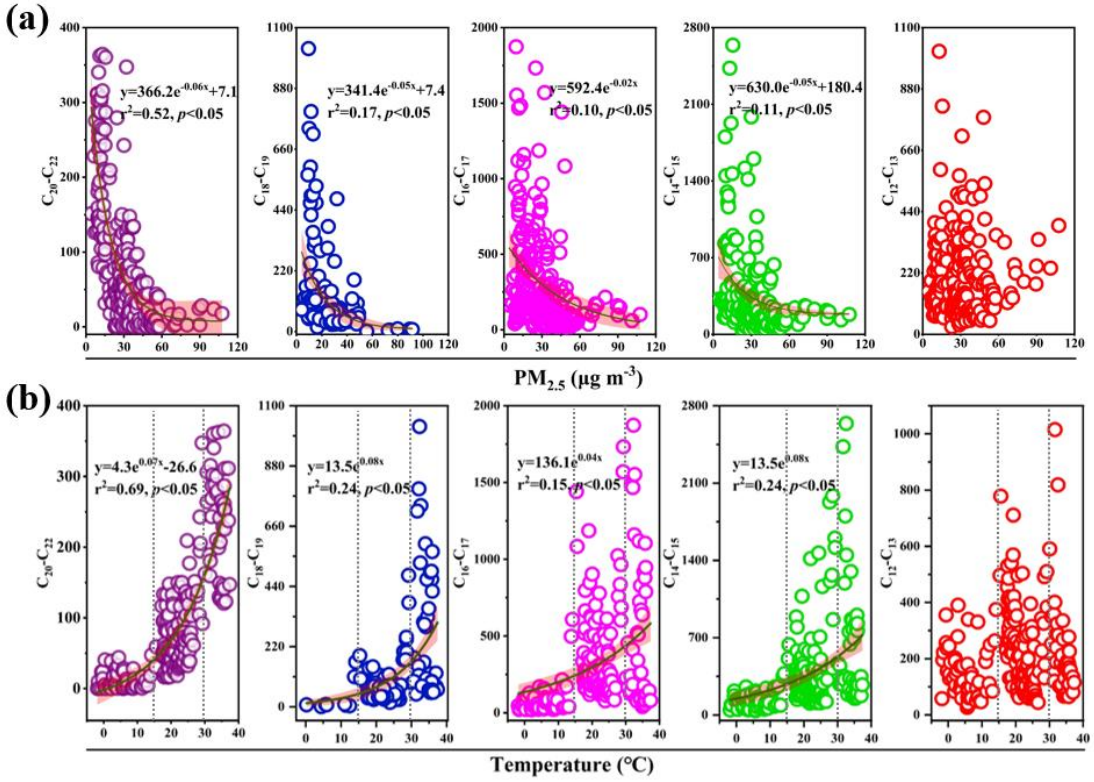


Figure 4. Concentrations of IVOCs (ng m^{-3}) in different volatility bins as a function of $PM_{2.5}$ levels (a) and ambient temperature (b). Shaded area represents 95% confidence interval.

In summary, seasonal variations of IVOC species were controlled by a temperature–volatility dual-control framework. Ambient temperature acted as a key modulator, simultaneously regulating temperature-dependent emission intensities and the dynamics of atmospheric processes. Moreover, IVOC volatility determined the dominant response mechanism: high-volatility IVOCs were controlled mainly by photochemical processes, whereas medium- and low-volatility fractions exhibited high sensitivity to temperature-dependent emission and gas/particle partitioning processes.

3.3 Source analysis

As summarized in Table S3, the carbon preference index (CPI) derived from our field samples was 0.86 ± 0.03 across the entire sampling period. Prior studies have established that CPI values of n-alkanes sourced from biogenic emissions typically exceed 2, whereas those from

petroleum-derived inputs cluster close to 1 (Mateus-Fontecha et al., 2022). On this basis, our results indicated that the measured IVOCs were predominantly from fossil fuel sources. The CPI exhibited pronounced seasonal variability, with the highest value recorded in winter (1.26 ± 0.25), followed by spring (0.91 ± 0.07), fall (0.87 ± 0.04), and summer (0.81 ± 0.06). This seasonal trend was attributable to shifts in the relative contributions of different emission sources across seasons. Combustion processes tend to yield higher CPI values compared to unburned fuels (Rogge et al., 1993; Zhu et al., 2005; Zhao et al., 2015, 2016). Elevated winter CPI coincided with a markedly strengthened correlation between IVOCs and CO, a tracer for incomplete combustion, in winter (Figure 5). Together, these observations indicated an enhanced contribution of combustion-derived sources to ambient IVOCs in cold winter. Whereas, the lower CPI values observed during warm seasons were likely driven by the amplified influence of evaporative emissions from unburned fossil fuels. Furthermore, strong correlations between IVOCs and both pristane (Pr) and phytane (Ph), two molecular tracers indicative of fossil sources inputs (Zhao et al., 2014; Chan et al., 2016), were consistently observed across all four seasons. This confirmed that petroleum-related sources represented a key contributor to the measured IVOCs.

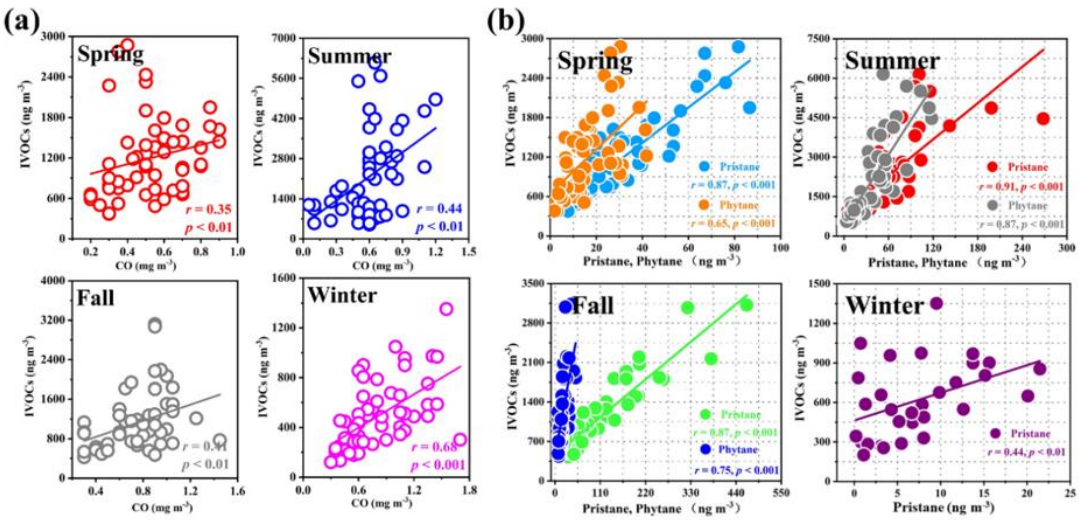


Figure 5. Correlations between total IVOCs and CO (a), and pristane and phytane (b) observed in four seasons.

3.4 Major contributing factors to observed IVOCs

To identify and quantify the specific contributors to the measured IVOCs, PMF model was applied in this study. As illustrated in Figure 6a, the PMF model resolved four dominant factors contributing to the measured IVOCs. It should be pointed out that the PMF factors resolved in this study included primary emission sources and an atmospheric process. Specifically, three of the factors represent direct emissions including vehicle exhaust, evaporative emissions, and industrial emissions, while the remaining one, gas/particle

partitioning, represents a critical atmospheric process that controls the phase distribution of measured IVOCs, particularly the low-volatility species. Factor 1 exhibited a pronounced abundance of nC_{12} – nC_{14}, consistent with the IVOC emission profiles previously reported for vehicle exhaust (Zhao et al., 2015, 2016; Fang et al., 2021a; Zhao et al., 2022; Zhang et al., 2024). In addition, elevated concentrations of combustion tracers such as CO, NO_2, and Nap further indicated the influence of combustion processes (Fang et al., 2021b). Therefore, Factor 1 was identified as vehicle exhaust. Factor 2 displayed high loadings of Pr and Ph, suggesting a linkage to petroleum-related contribution. However, the extremely low levels of CO, NO_2, and Nap implied a non-combustion origin. The factor was consequently attributed to evaporative emissions. This interpretation was also corroborated by a statistically significant positive correlation ($p < 0.05$, Figure S7) between the IVOCs in Factor 2 and isopentane. Furthermore, the IVOCs apportioned to Factor 2 showed a clear correlation with ambient temperature (Figure S8), supporting its identification as a temperature-dependent evaporative emission. Moreover, evaporative IVOCs are also from asphalt (itself petroleum-derived) and volatile chemical products (VCPs) (McDonald et al., 2018; Khare et al., 2020; Wan et al., 2026). PMF model cannot further sub-partition this factor to separate contributions from fuel evaporation, asphalt, and VCPs. Therefore, Factor 2 resolved by PMF was primarily attributed to bulk evaporative emissions, with fuel evaporation as the important constrained contributor, based on its significant correlations with isopentane, Pr, and Ph. Factor 3 was also characterized by minimal CO and NO_2 levels, indicating a non-combustion contributor. Notably, this factor was dominated by low-volatility nC_{19} – nC_{22}, which are susceptible to phase transfer. Furthermore, the IVOCs attributed to Factor 3 exhibited a strong positive correlation with temperature ($r = 0.79$, $p < 0.01$, Figure S9), consistent with the temperature-driven repartitioning of low-volatility organics from the particle phase to the gas phase (Zhou et al., 2024). This factor also showed a pronounced exponential decay with increasing $PM_{2.5}$ concentrations, reflecting the condensation sink effect under high aerosol loading. Hence, Factor 3 was interpreted as reflecting gas/particle partitioning processes, rather than a conventional primary source. Factor 4 was characterized by significant amount of SO_2, CO, and NO_2, which are typical industrial pollutants (Klimont et al., 2013; Plauchu et al., 2024). The IVOCs apportioned to this factor also showed a strong correlation with SO_2 (Figure S10), further confirming the assignment of this factor to industrial emissions.

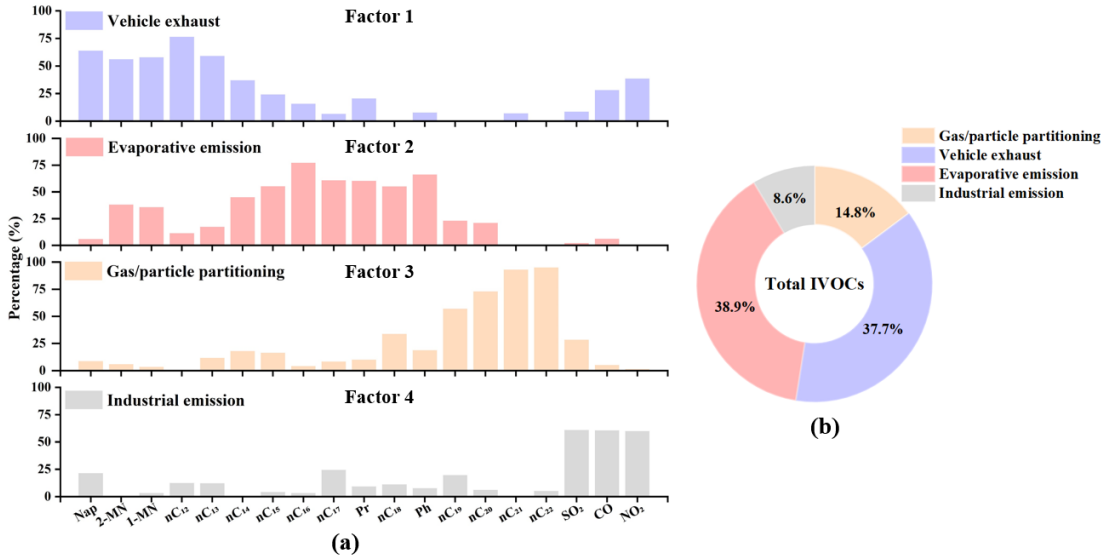


Figure 6. Factor profiles (% of the species) resolved by PMF (a) and relative contributions of various factors to measured IVOCs (b).

Figure 6b shows the relative contributions of four resolved factors to measured IVOCs. Evaporative emission emerged as the predominant contributor, accounting for 38.9% of the total measured IVOCs. As Figure S11 shows, the contribution of this factor exhibited pronounced seasonal variation, being the highest in hot summer (59.2%) and the lowest in cold winter (22.0%). The dominance of evaporative emissions aligned with a recent growing body of evidence underscoring their importance in the anthropogenic emissions. For example, Porada et al. (2016) demonstrated that fuel evaporation exceeded tailpipe exhaust as a source of VOCs in North America. Similarly, Yan et al. (2021) recently quantified that evaporative emission contributed 73% of total vehicle-related VOCs in China, in contrast to 27% from tailpipe exhaust. While the significance of evaporative emission for VOCs is increasingly recognized, their specific contribution to IVOCs remains poorly quantified in both field observations and emission inventories. Previous studies revealed that despite their relatively lower emission than VOCs, IVOCs from gasoline evaporation exhibited comparable ozone formation potential to that of VOCs, and their SOA formation (58%) even exceeded that of VOCs (42%) (Yang et al., 2024; Wang et al., 2025). Beyond fuel evaporation, asphalt and VCP have recently been revealed to contribute evaporative IVOCs in the real atmosphere (Khare et al., 2020; Lasne et al., 2023; Wang et al., 2024). Asphalt-based materials, used extensively in road paving and roofing, consist of approximately 85% I/SVOCs (Lasne et al., 2023), and have been found to emit substantial organic vapor, particularly at elevated temperatures and from aged asphalt (Khare et al., 2020). Given China's substantial annual asphalt consumption (e.g., 21.5 million tons in 2024, with over 90% used for road paving and roofing, https://www.yunliqing.com/public//static/uploads/files/pdf/2024/12/19/17345905736

763c06debf64.pdf), this may represent a significant and sustained contributor to evaporative IVOCs in urban areas. Moreover, emission inventories have identified VCPs as the dominant contributor to ambient IVOCs in China, accounting for 32.4% ± 4.9% of IVOC emissions from 2005 to 2019 (Zheng et al., 2023). In contrast to the significant progress in reducing traditional anthropogenic sources like vehicular and industrial emissions, evaporative sources (e.g., fuel evaporation, asphalt-related emission, and VCP), especially for IVOCs, have been challenging to quantify and remain largely uncontrolled. It was worth noting that these IVOC species are not yet explicitly considered in China's current air quality management policies. Given the strong temperature dependence of evaporative emission, rising global temperatures and frequent heatwaves are projected to significantly enhance the amounts of evaporative IVOCs in real atmospheres. As a result, uncontrolled evaporative emission may increasingly offset achievements in reducing traditional anthropogenic source emission, and increase urban background level of IVOCs.

Vehicle exhaust was the second-largest contributor, accounting for 37.7% of measured IVOCs. Unlike the temperature-dependent evaporative emission, vehicular contribution peaked in the cold winter (Figure S11). This seasonal pattern was supported by stronger positive correlation observed between IVOCs and combustion tracer (CO, Figure 5a) in winter, as well as by a significant negative correlation between the vehicular IVOC fraction and ambient temperature ($r = -0.43$, $p < 0.01$; Figure S12). The elevated wintertime concentrations of vehicular IVOCs were likely attributable to enhanced incomplete combustion and reduced catalytic converter efficiency under cold temperature conditions, both of which could enlarge IVOC emissions from vehicles (Zhao et al., 2018; Wu et al., 2025a). Vehicle exhaust has been previously reported as an important contributor to ambient IVOCs in urban China. Based on top-down observations and bottom-up emission inventories, vehicle exhaust accounted for 10% – 30% of atmospheric IVOCs in China (Wu et al., 2021b; Chang et al., 2022; Cui et al., 2022; Fang et al., 2022; Tong et al., 2024). However, stricter vehicular emission standards have significantly cut IVOC emissions, albeit these regulations were not originally designed for such purpose. For instance, Qi et al. (2021) reported a 77.6% decrease in the IVOC emission factor from China II to China V gasoline vehicles. Furthermore, advanced after-treatment technologies have reduced IVOC emissions by a factor of 28 for diesel vehicles and 1.8 − 55.6 for gasoline vehicles (Zhao et al., 2015; Tang et al., 2024). These findings suggested that the contribution of vehicle exhaust to atmospheric IVOCs is expected to decline further with the continued modernization of vehicle fleets and emission control technologies.

Gas/particle partitioning explained 14.8% of the measured IVOCs (Figure 6b). This process predominantly influenced the low-volatility IVOCs (nC_{19} − nC_{22}), promoting their volatilization from the particle phase under warm condition, elevating their gas-phase concentrations. Thus, these gaseous species were rarely detected in the cold winter in this

study (Figure 3). As shown in Figure S9, the IVOCs apportioned to this factor was highly temperature-dependent ($r = 0.79$, $p < 0.01$), leading to higher contributions in warmer seasons (Figure S11). In view of the strong temperature dependence governing gas/particle partitioning, ongoing global warming is projected to further shift these low-volatility IVOCs towards the gas phase. In addition, the effective control of particulate pollution in China (Zheng et al., 2025) will reduce the available particle phase, thereby releasing more particle-bound IVOCs into the gas phase. Such a phase redistribution would alter their atmospheric fate and may enhance the role of gas-phase chemistry of IVOCs in future.

From Figure 6b, industrial emissions made a minor contribution (8.6%) to the measured IVOCs. This contribution increased in cold winter, followed by spring, fall, and summer, as showed in Figure S11. Previous field observation also identified industrial emissions as a non-dominant contributor to atmospheric IVOCs. Even within industrial parks, industrial emission contributed less to IVOCs than combustion sources (19.5% vs. 61.5%) (Hou et al., 2026). A recent emission inventory revealed that industrially-emitted IVOCs have decreased significantly in China since 2015, accounting for less than 8% of total IVOCs during 2015−2019 (Zheng et al., 2023). However, some earlier emission inventory studies have reported a substantial contribution from industrial emission to atmospheric IVOCs. Several factors may explain this apparent discrepancy. For example, earlier inventories often estimated IVOC emissions using ratios relative to other air pollutants (e.g., VOCs, POA, and Nap), an approach known to introduce considerable uncertainty (Lu et al., 2020; Yang et al., 2025). Additionally, industrial-related IVOCs could be dominated by other IVOC species such as oxygenated species (Liang et al., 2024; Yang et al., 2024) rather than the hydrocarbon IVOCs measured in this study. Therefore, more IVOC species need to be identified and quantified in future to comprehensively understand industrial contribution to ambient IVOCs.

4. Conclusions and implications

This study performed field observations at an urban site in the Yangtze River Delta (YRD) to systematically investigate seasonal patterns of primary IVOCs and the key drivers behind their variations. Results showed that the total concentration of measured IVOCs was 1228.2 ± 132.7 ng m^{-3}, with long-chain alkanes as the dominant component. In contrast to typical primary air pollutants, IVOCs exhibited a distinct seasonal pattern characterized by a summer maximum and winter minimum. This pattern was driven by enhanced temperature-dependent evaporative emissions during warm seasons. Concurrently, gas/particle partitioning process also exerted a pivotal regulatory role in the seasonal variations of low-volatility IVOCs, which almost entirely sequestered in particles during the cold winter but re-volatilized into the gas phase in warm seasons. Petroleum-related sources were identified as key contributors to the measured IVOCs. Positive matrix factorization (PMF) resolved four contributors: evaporative emissions (38.9%), vehicle exhaust (37.7%), gas/particle partitioning (14.8%),

and industrial emissions (8.6%).

Our results highlight that temperature-dependent evaporative emissions and gas/particle partitioning are the core drivers of the seasonal cycle of ambient IVOCs. This mechanistic insight is critical for the accurate parameterization of regional secondary organic aerosol (SOA) formation models. The predominance of evaporative emissions and their strong temperature dependence indicate that these unregulated sources are emerging as dominant contributors to urban IVOC loads, particularly in warm seasons, given that regulatory measures have effectively mitigated combustion-related emissions (Khare et al., 2018; Zhao et al., 2024b). Under future global warming scenarios, intensified evaporative emissions may substantially elevate urban background IVOC concentrations. This may offset some of the air quality gains achieved through controls on traditional anthropogenic sources (e.g., vehicular and industrial emissions). Notably, such evaporative emissions are not currently incorporated into Chinese IVOC emission inventories (Zheng et al., 2023). Thus, integrating evaporative IVOCs into emission inventories and regulatory frameworks is indispensable for sustained air quality improvements. Furthermore, ongoing climate warming and continuing declines in aerosol concentrations across urban China are projected to amplify the gas/particle partitioning process of IVOCs, especially low-volatility species, shifting them more prominently toward the gas phase. This phase redistribution may fundamentally alter the atmospheric chemistry of IVOCs, underscoring the need for long-term ambient IVOC observations to constrain these dynamic processes. Additionally, this study focused on 16 representative hydrocarbon IVOC species. The reported concentrations and PMF-resolved relative contributions are therefore specific to these measured compounds and cannot fully capture the entire atmospheric IVOC pool. Nevertheless, our findings regarding temperature-dependent evaporation and gas/particle partitioning are generalizable to the broader IVOC continuum, since the measured compounds span the IVOC volatility window. Although current work conducted a case study at an urban site in the YRD, evaporative processes are believed to occur widely in urban areas. Therefore, their contributions to ambient IVOCs is equally important for other cities. Future multi-site and long-term observations covering a broader suite of IVOC species are recommended to better generalize seasonal patterns and quantitatively delineate evaporation contributions to regional IVOC budgets.

Acknowledgments

The authors gratefully acknowledge the support from National Natural Science Foundation of China, the State Key Laboratory of Advanced Environmental Technology, and Anhui Normal University.

Financial support

This work has been funded by the National Natural Science Foundation of China (42207128), Open Fund of the State Key Laboratory of Advanced Environmental Technology (SKLAET202507), and National College Student Innovation and Entrepreneurship Training Program Support Project (202510370775, 202510370785).

Conflict of Interest

The authors declare no conflicts of interest relevant to this study.

Data Availability Statement

Measured data used in this study can be found at https://data.mendeley.com/datasets/8rx9c3nr4p/1.

Author contributions

HF designed the experiments, analyzed the data, and wrote the paper. HX, JL, QJ, SM, XD, and HB collected and analyzed the samples. FX provided suggestions for this work. WT and XW provided suggestions for the study and revised the manuscript.

References

Ait-Helal, W., Borbon, A., Sauvage, S., de Gouw, J. A., Colomb, A., Gros, V., Freutel, F., Crippa, M., Afif, C., Baltensperger, U., Beekmann, M., Doussin, J. F., Durand-Jolibois, R., Fronval, I., Grand, N., Leonardis, T., Lopez, M., Michoud, V., Miet, K., Perrier, S., Prévôt, A. S. H., Schneider, J., Siour, G., Zapf, P., and Locoge, N.: Volatile and intermediate volatility organic compounds in suburban Paris: variability, origin and importance for SOA formation, Atmos. Chem. Phys., 14, 10439–10464, https://doi.org/10.5194/acp-14-10439-2014, 2014.

An, T.K., Li, Y.J., Wang, R., Jing, S.A., Gao, Y.Q., Liu, S.Y., Huang, D.D., Zhou, M., Dai, H.X., Huang, C., Lu, J., Wang, H.L., and Fu, Q.Y.: Characteristics of typical intermediate and semi-volatile organic compounds in Shanghai during the China International Import Expo Event, Chemosphere. 355, 141779, https://doi.org/10.1016/j.chemosphere.2024.141779, 2024.

Chan, A.W.H., Kreisberg, N.M., Hohaus, T., Campuzano-Jost, P., Zhao, Y., Day, D.A., Kaser, L., Karl, T., Hansel, A., Teng, A.P., Ruehl, C.R., Sueper, D.T., Jayne, J.T., Worsnop, D.R., Jimenez, J.L., Hering, S.V., and Goldstein, A.H.: Speciated measurements of semivolatile and intermediate volatility organic compounds (S/IVOCs) in a pine forest during BEACHON-RoMBAS 2011, Atmos. Chem. Phys., 16, 1187–1205, https://doi.org/10.5194/acp-16-1187-2016, 2016

Chang, X., Zhao, B., Zheng, H., Wang, S., Cai, S., Guo, F., Gui, P., Huang, G., Wu, D., Han, L., Xing, J., Man, H., Hu, R., Liang, C., Xu, Q., Qiu, X., Ding, D., Liu, K., Han, R., Robinson, A.L., and Donahue, N.M.: Full-volatility emission framework corrects missing and underestimated secondary organic aerosol sources, One Earth. 5, 403–412,

https://doi.org/10.1016/j.oneear.2022.03.015, 2022.

Chen, Y., Xia, M., Zheng, P.G., Li, Y.M., Zou, Z.X., Tong, S.R., Li, K., Feng, X., Hui, L.R., Yuan, Q., Li, J.J., Yu, J.Z., Lee, S.C., Wang, T., and Wang, Z.: Complex gas-particle partitioning of nitro-phenolic compounds: field-based insights and determination of apparent activity coefficient, npj Clim. Atmos. Sci., 8, 266, https://doi.org/10.1038/s41612-025-01156-z, 2025.

Cui, M., Hou, X.X., Han, Y.X., Zhang, Y.S., Liu, Z.Y., Li, J., Chen, Y.J., Zhang, F., Yan, C.Q., and Zhang, Y.: Real-world emissions and formation mechanism of IVOCs from biodiesel-fueled agricultural machinery, Environ. Sci. Technol., 59, 9017–9026, https://doi.org/10.1021/acs.est.4c11004, 2025.

Donahue, N.M., Kroll, J.H., Pandis, S.N., and Robinson, A.L.: A two-dimensional volatility basis set – Part 2: Diagnostics of organic-aerosol evolution, Atmos. Chem. Phys., 12, 615–634, https://doi.org/10.5194/acp-12-615-2012, 2012.

Drozd, G.T., Zhao, Y.L., Saliba, G., Frodin, B., Maddox, C., Oliver Chang, M.C., Maldonado, H., Sardar, S., Weber, R.J., Robinson, A.L., and Goldstein, A.H.: Detailed speciation of intermediate volatility and semivolatile organic compound emissions from gasoline vehicles: effects of cold-starts and implications for secondary organic aerosol formation. Environ. Sci. Technol., 53, 1706–1714, https://doi.org/10.1021/acs.est.8b05600, 2019.

Fang, H., Huang, X.Q., Xiao, S.X., Lowther, S., Fu, X.W., Zhang, Y.L., Wu, T., Hu, W.W., Zhang, G.H., Ding, X., Tang, M.J., Bi, X.H., Jones, K.C., and Wang, X.M.: Intermediate-volatility organic compounds observed in a coastal megacity: Importance of non-road source emissions, J. Geophys. Res. Atmos., 127, e2022JD037301, https://doi.org/10.1029/2022JD037301, 2022.

Fang, H., Huang, X.Q., Zhang, Y.L., Pei, C.L., Huang, Z.Z., Wang, Y.J., Chen, Y.N., Yan, J.H., Zeng, J.Q., Xiao, S.X., Luo, S.L., Li, S., Wang, J., Zhu, M., Fu, X.W., Wu, Z.F., Zhang, R.Q., Song, W., Zhang, G.H., Hu, W.W., Tang, M.J., Ding, X., Bi, X.H., and Wang, X.M.: Measurement report: emissions of intermediate-volatility organic compounds from vehicles under real-world driving conditions in an urban tunnel, Atmos. Chem. Phys., 21, 10005–10013, https://doi.org/10.5194/acp-21-10005-2021, 2021a.

Fang, H., Lowther, S., Zhu, M., Pei, C.L., Li, S., Fang, Z., Yu, X., Yu, Q.Q., Wang, Y.J., Zhang, Y.L., Jones, K.C., and Wang, X.M.: $PM_{2.5}$-bound unresolved complex mixtures (UCM) in the Pearl River delta region: abundance, atmospheric processes and sources, Atmos. Environ., 226, 117407, https://doi.org/10.1016/j.atmosenv.2020.117407, 2020.

Fang, H., Luo, S.L., Huang, X.Q., Fu, X.W., Xiao, S.X., Zeng, J.Q., Wang, J., Zhang, Y.L., and Wang, X.M.: Ambient naphthalene and methylnaphthalenes observed at an urban site in the Pearl River Delta region: sources and contributions to secondary organic aerosol, Atmos. Environ., 252, 118295, https://doi.org/10.1016/j.atmosenv.2021.118295,

627 2021b.
628 Galeazzo, T., Aumont, B., Camredon, M., Valorso, R., Lim, Y.B., Ziemann, P.J., and Shiraiwa,
629 M.: Secondary organic aerosols derived from intermediate-volatility n-alkanes adopt
630 low-viscous phase state, Atmos. Chem. Phys., 24, 5549–5565,
631 https://doi.org/10.5194/acp-24-5549-2024, 2024.
632 Gou, Y.F., Qin, C., Liao, H., and Xie, M.J.: Measurements, gas/particle partitioning, and
633 sources of nonpolar organic molecular markers at a suburban site in the west Yangtze
634 River Delta, China, J. Geophys. Res. Atmos., 126, e2020JD034080,
635 https://doi.org/10.1029/2020JD034080, 2021.
636 Hodzic, A., Kasibhatla, P.S., Jo, D.S., Cappa, C.D., Jimenez, J.L., Madronich, S., and Park,
637 R.J.: Rethinking the global secondary organic aerosol (SOA) budget: stronger production,
638 faster removal, shorter lifetime, Atmos. Chem. Phys., 16, 7917–7941,
639 https://doi.org/10.5194/acp-16-7917-2016, 2016.
640 Hou, X.X., Chen, Y.J., Zhuang, W.T., Shi, F. Q., Zhang, Y.S., Yan, C.Q., and Cui, M.:
641 Spatiotemporal characteristics and source apportionment of intermediate volatility
642 organic compounds in the riverside industrial parks, Environ. Pollut., 388, 127361,
643 https://doi.org/10.1016/j.envpol.2025.127361, 2026.
644 Huang, C., Hu, Q.Y., Li, Y.J., Tian, J.J., Ma, Y.G., Zhao, Y.L., Feng, J.L., An, J.Y., Qiao, L.P.,
645 Wang, H.L., Jing, S.A., Huang, D.D., Lou, S.R., Zhou, M., Zhu, S.H., Tao, S.K., and Li,
646 L.: Intermediate volatility organic compound emissions from a large cargo vessel
647 operated under real-world conditions, Environ. Sci. Technol., 52, 12934–12942,
648 https://doi.org/10.1021/acs.est.8b04418, 2018.
649 Huang, G.C., Liu, Y., Shao, M., Li, Y., Chen, Q., Zheng, Y., Wu, Z.J., Liu, Y.C., Wu, Y.S., Hu,
650 M., Li, X., Lu, S.H., Wang, C.J., Liu, J.Y., Zheng, M., and Zhu, T.: Potentially important
651 contribution of gas-phase oxidation of naphthalene and methylnaphthalene to secondary
652 organic aerosol during haze events in Beijing, Environ. Sci. Technol., 53, 1235–1244,
653 https://doi.org/10.1021/acs.est.8b04523, 2019.
654 Khare, P., and Gentner, D.R.: Considering the future of anthropogenic gas-phase organic
655 compound emissions and the increasing influence of non-combustion sources on urban
656 air quality, Atmos. Chem. Phys., 18, 5391–5413,
657 https://doi.org/10.5194/acp-18-5391-2018, 2018.
658 Khare, P., Machesky, J., Soto, R., He, M., Presto, A.A., and Gentner, D.R.: Asphalt-related
659 emissions are a major missing nontraditional source of secondary organic aerosol
660 precursors, Sci. Adv., 6, eabb9785, https://doi.org/10.1126/sciadv.abb9785, 2020.
661 Klimont, Z., Smith, S.J., and Cofala, J.: The last decade of global anthropogenic sulfur
662 dioxide: 2000–2011 emissions. Environ. Res. Lett., 8, 014003,
663 https://doi.org/10.1088/1748-9326/8/1/014003, 2013.

Kong, M.D., Hao, Y.Y., Xu, R.X., Guo, J., Wei, X.F., Yin, S.S., and Zhang, R.Q.: Characteristic trends and source shifts of n-alkanes in a multi-year study: insights from gas-particle partitioning in a central Chinese city. J. Hazard. Mater., 488, 137445, https://doi.org/10.1016/j.jhazmat.2025.137445, 2025.

Lasne, J., Lostier, A., Romanias, M.N., Vassaux, S., Lesueur, D., Gaudion, V., Jamar, M., Derwent, R.G., Dusanter, S., and Salameh, T.: VOC emissions by fresh and old asphalt pavements at service temperatures: impacts on urban air quality. Environ. Sci. Atmos., 3, 1601−1619, https://doi.org/10.1039/D3EA00034F, 2023.

Li, J.L., Li, K., Li, H., Wang, X.Z., Wang, W.G., Wang, K., and Ge, M.F.: Long-chain alkanes in the atmosphere: a review. J. Environ. Sci., 114, 37-54, https://doi.org/10.1016/j.jes.2021.07.021, 2022.

Li, Y.J., Ren, B.N., Qiao, Z., Zhu, J., Wang, H., Zhou, M., Qiao, L.P., Lou, S.R., Jing, S.G., Huang, C., Tao, S.K., Rao, P.H., and Li, J.: Characteristics of atmospheric intermediate volatility organic compounds (IVOCs) in winter and summer under different air pollution levels. Atmos. Environ., 210, 58–65, https://doi.org/10.1016/j.atmosenv.2019.04.041, 2019.

Li. J., Han, Z.W., Sun, Y.L., Li, J.W., and Liang, L.: Chemical formation pathways of secondary organic aerosols in the Beijing-Tianjin-Hebei region in wintertime. Atmos. Environ., 244, 117996, https://doi.org/10.1016/j.atmosenv.2020.117996, 2021.

Liang, C.R., Feng, B.Y., Wang, S.X., Zhao, B., Xie, J.Z., Huang, G.H., Zhu, L., and Hao, J.M.: Differentiated emissions and secondary organic aerosol formation potential of organic vapor from industrial coatings in China. J. Hazard. Mater., 466, 133668, https://doi.org/10.1016/j.jhazmat.2024.133668, 2024.

Ling, Z.H., Wu, L.Q., Wang, Y.H., Shao, M., Wang, X.M., and Huang, W.W.: Roles of semivolatile and intermediate-volatility organic compounds in secondary organic aerosol formation and its implication: a review. J. Environ. Sci., 114, 259-285, https://doi.org/10.1016/j.jes.2021.08.055, 2022.

Liu, Z.Y., Chen, Y.J., Zhang, Y., Zhang, F., Feng, Y.L., Zheng, M., Li, Q., and Chen, J.M.: Emission characteristics and formation pathways of intermediate volatile organic compounds from ocean-going vessels: comparison of engine conditions and fuel types. Environ. Sci. Technol., 56, 12917–12925, https://doi.org/10.1021/acs.est.2c03589, 2022.

Lu, Q., Murphy, B. N., Qin, M., Adams, P. J., Zhao, Y., Pye, H.O.T., Efstathiou, C., Allen, C., and Robinson, A.L.: Simulation of organic aerosol formation during the CalNex study: updated mobile emissions and secondary organic aerosol parameterization for intermediate-volatility organic compounds. Atmos. Chem. Phys., 20, 4313–4332, https://doi.org/10.5194/acp-20-4313-2020, 2020.

Lumiaro, E., Todorović, M., Kurten, T., Vehkamäki, H., and Rinke, P.: Predicting gas–particle

partitioning coefficients of atmospheric molecules with machine learning. Atmos. Chem. Phys., 21, 13227–13246, https://doi.org/10.5194/acp-21-13227-2021, 2021.

Manavi, S.E. I., and Pandis, S.N.: A lumped species approach for the simulation of secondary organic aerosol production from intermediate-volatility organic compounds (IVOCs): application to road transport in PMCAMx-iv (v1.0). Geosci. Model Dev., 15, 7731–7749, https://doi.org/10.5194/gmd-15-7731-2022, 2022.

Mateus-Fontecha, L., Vargas-Burbano, A., Jimenez, R., Rojas, N.Y., Rueda-Saa, G., van Pinxteren, D., van Pinxteren, M., Fomba, K.W., and Herrmann, H.: Understanding aerosol composition in a tropical inter-Andean valley impacted by agro-industrial and urban emissions. Atmos. Chem. Phys., 22, 8473–8495, https://doi.org/10.5194/acp-22-8473-2022, 2022.

McDonald, B.C., de Gouw, J.A., Gilman, J.B., Jathar, S.H., Akherati, A., Cappa, C.D., Jimenez, J.L., Lee-Taylor, J., Hayes, P.L., McKeen, S.A., Cui, Y.Y., Kim, S.W., Gentner, D.R., Isaacman-VanWertz, G., Goldstein, A.H., Harley, R.A., Frost, G.J., Roberts, J.M., Ryerson, T.B., and Trainer, M.: Volatile chemical products emerging as largest petrochemical source of urban organic emissions. Science, 359, 760–764, https://doi.org/10.1126/science.aaq0524, 2018.

Pennington, E.A., Seltzer, K.M., Murphy, B.N., Qin, M., Seinfeld, J.H., and Pye, H.O.T.: Modeling secondary organic aerosol formation from volatile chemical products. Atmos. Chem. Phys., 21, 18247–18261, https://doi.org/10.5194/acp-21-18247-2021, 2021.

Plauchu, R., Fortems-Cheiney, A., Broquet, G., Pison, I., Berchet, A., Potier, E., Dufour, G., Coman, A., Savas, D., Siour, G., and Eskes, H.: NOx emissions in France in 2019–2021 as estimated by the high-spatial-resolution assimilation of TROPOMI NO_2 observations. Atmos. Chem. Phys., 24, 8139–8163, https://doi.org/10.5194/acp-24-8139-2024, 2024.

Porada, E., and Szyszkowicz, M.: UNMIX methods applied to characterize sources of volatile organic compounds in Toronto, Ontario. Toxics., 4, 11, https://doi.org/10.3390/toxics4020011, 2016.

Presto, A.A., Hennigan, C.J., Nguyen, N.T., and Robinson, A.L.: Determination of volatility distributions of primary organic aerosol emissions from internal combustion engines using thermal desorption gas chromatography mass spectrometry. Aerosol Sci. Technol., 46, 1129–1139, https://doi.org/10.1080/02786826.2012.700430, 2012.

Pye, H.O.T., and Seinfeld, J.H.: A global perspective on aerosol from low-volatility organic compounds. Atmos. Chem. Phys., 10, 4377–4401, https://doi.org/10.5194/acp-10-4377-2010, 2010.

Qi, L.J., Zhao, J.C., Li, Q.W., Su, S., Lai, Y.T., Deng, F.Y., Man, H.Y., Wang, X.T., Shen, X.E., Lin, Y.M., Ding, Y., and Liu, H.: Primary organic gas emissions from gasoline vehicles in China: factors, composition and trends. Environ. Pollut., 290, 117984,

https://doi.org/10.1016/j.envpol.2021.117984, 2021.

Qian, Z., Chen, Y.J., Liu, Z.Y., Han, Y., Zhang, Y.S., Feng, Y.L., Shang, Y., Guo, H., Li, Q., Shen, G.F., Chen, J.M., and Tao, S.: Intermediate volatile organic compound emissions from residential solid fuel combustion based on field measurements in rural China. Environ. Sci. Technol., 55, 5689−5700, https://doi.org/10.1021/acs.est.0c07908, 2021.

Robinson, A.L., Donahue, N.M., Shrivastava, M.K., Weitkamp, E.A., Sage, A.M., Grieshop, A.P., Lane, T.E., Pierce, J.R., and Pandis, S.N.: Rethinking organic aerosols: semivolatile emissions and photochemical aging. Science 315, 1259–1262, https://doi.org/10.1126/science.1133061, 2007.

Rogge, W., Hildemann, L.M., Mazurek, M.A., Cass, G.R., and Simoneit, B.R.T.: Sources of fine organic aerosol. 2. Noncatalyst and catalyst-equipped automobiles and heavy-duty diesel trucks. Environ. Sci. Technol., 27, 636−651, https://doi.org/10.1021/es00041a007, 1993.

Scholz, S. M.C., Karydis, V.A., Gkatzelis, G.I., Fuchs, H., Pandis, S.N., and Tsimpidi, A.P.: Incorporation of lumped IVOC emissions into the ORACLE model (V1.1): a multi-product framework for assessing global SOA formation from internal combustion engines. Geosci. Model Dev., 18, 10119–10142, https://doi.org/10.5194/gmd-18-10119-2025, 2025.

Tang, R.Z., Guo, S., Lu, Q.Y., Song, K., Gong, Y.Z., Tan, R., Liu, K.F., Wang, H., Yu, Y., Shen, R.Z., Chen, S.Y., Zeng, L.M., Jorga, S. D., and Robinson, A. L.: Unexpected moderate contribution of intermediate volatility organic compounds from gasoline vehicle emission to secondary organic aerosol formation in summer of Beijing. Atmos. Res., 295, 106990, https://doi.org/106990. 10.1016/j.atmosres.2023.106990, 2023.

Tang, R.Z., Guo, S., Song, K., Yu, Y., Tan, R., Wang, H., Liu, K.F., Shen, R.Z., Chen, S.Y., Zeng, L.M., Zhang, Z., Zhang, W.B., Shuai, S.J., and Hu, M.: Emission characteristics of intermediate volatility organic compounds from a Chinese gasoline engine under varied operating conditions: Influence of fuel, velocity, torque, rotational speed, and after-treatment device. Sci. Total. Environ., 906, 167761, https://doi.org/10.1016/j.scitotenv.2023.167761, 2024.

Tang, R.Z., Lu, Q.Y., Guo, S., Wang, H., Song, K., Yu, Y., Tan, R., Liu, K.F., Shen, R.Z., Chen, S.Y., Zeng, L.M., Jorga, S. D., Zhang, Z., Zhang, W.B., Shuai, S.J., and Robinson, A. L.: Measurement report: distinct emissions and volatility distribution of intermediate-volatility organic compounds from on-road Chinese gasoline vehicles: implication of high secondary organic aerosol formation potential. Atmos. Chem. Phys., 21, 2569−2583, https://doi.org/10.5194/acp-21-2569-2021, 2021.

Tang, T.G., Cheng, Z.N., Xu, B.Q., Zhang, B.L., Li, J., Zhang, W., Wang, K.L., and Zhang, G.: Source diversity of intermediate volatility n-alkanes revealed by compound-specific

775 $\delta^{13}C-\delta D$ isotopes. Environ. Sci. Technol., 56, 14262–14271,
776 https://doi.org/10.1021/acs.est.2c02156, 2022.
777 Tang, T.G., Cheng, Z.N., Xu, B.Q., Zhang, B.L., Zhu, S.Y., Cheng, H.R., Li, J., Chen, Y.J.,
778 and Zhang, G.: Triple isotopes ($\delta^{13}C$, $\delta^{2}H$, and $\Delta^{14}C$) compositions and source
779 apportionment of atmospheric naphthalene: a key surrogate of intermediate-volatility
780 organic compounds (IVOCs). Environ. Sci. Technol., 54, 5409–5418,
781 https://doi.org/10.1021/acs.est.0c00075, 2020.
782 Tanzer-Gruener, R., Rajan, P.E., Dugan, L.D., Bier, M.E., Robinson, A.L., and Presto, A.A.:
783 Watching paint dry: organic vapor emissions from architectural coatings and their impact
784 on secondary organic aerosol formation. Environ. Sci. Technol., 56, 11236–11245,
785 https://doi.org/10.1021/acs.est.2c02478, 2022.
786 Tong, M.X., Zhang, Y.L., Xiao, S.X., Pei, C.L., Wang, J., Zhang, R.Q., Huang, X.Q., Song,
787 W., and Wang, X.M.: Role of organic vapor precursors in secondary organic aerosol
788 formation: concurrent observations of IVOCs and VOCs in Guangzhou. J. Geophys. Res.:
789 Atmos., 129, e2024JD041018, https://doi.org/10.1029/2024JD041018, 2024.
790 Wang, Q.Q., Feng, Y.M., Huang Hilda, X.H., Griffith, S.M., Zhang, T., Zhang, Q.Y., Wu, D.,
791 and Yu, J.Z.: Nonpolar organic compounds as $PM_{2.5}$ source tracers: investigation of their
792 sources and degradation in the Pearl River Delta, China. J. Geophys. Res. Atmos., 121,
793 11862–11879, https://doi.org/10.1002/2016JD025315, 2016.
794 Wang, Y., Li, X., Kong, L.W., Lu, S.H., Liu, Y., Dou, X.Y., Wang, K., Wang, F., Shi, X.C.,
795 Wang, J., Zou, Y., Lian, C.F., and Zhang, Y.H.: Emission characteristics of evaporative
796 intermediate-volatility organic compounds from in-use gasoline vehicles. Environ. Sci.
797 Technol., 59, 13730–13741, https://doi.org/10.1021/acs.est.5c06497, 2025.
798 Wang, Y.J., Huang, J.Y., Zhao, B., Du, Y.F., Huang, L., Lai, D.M., Su, Q.F., Manomaiphiboon,
799 K., and Li, L.: Full-volatility reactive organic carbon emissions from volatile chemical
800 products in mainland China. ACS ES&T Air., 1, 1541−1553,
801 https://doi.org/10.1021/acsestair.4c00116, 2024.
802 Wan, Z.C., Guo, S., Ni, X.S., Zhou, Q.Q., Hu, K., Chen, S.Y., Yao, M.S., and Donahue, N.M.:
803 Urban activity shifts reshape S/IVOC composition and SOA formation: insights from
804 wintertime observations in Beijing, Environ. Sci. Technol., 60, 17927-17937,
805 https://doi.org/10.1021/acs.est.5c17863, 2026.
806 Wernis, R.A., Kreisberg, N.M., Weber, R.J., Drozd, G.T., and Goldstein, A.H.: Source
807 apportionment of VOCs, IVOCs and SVOCs by positive matrix factorization in
808 suburban Livermore, California. Atmos. Chem. Phys., 22, 14987–15019,
809 https://doi.org/10.5194/acp-22-14987-2022, 2022.
810 Wu, L.Q., Lin, Z.H., Shao, M., Liu, H., Lu, S.H., Zhou, S.Z., Guo, J.C., Mao, J.Y., Hang, J.,
811 and Wang, X.M.: Roles of semivolatile/intermediate-volatility organic compounds on

SOA formation over China during a pollution episode: sensitivity analysis and implications for future studies. J. Geophys. Res.: Atmos., 126, e2020JD033999, https://doi.org/10.1029/2020JD033999, 2021a.

Wu, L.Q., Ling, Z.H., Liu, H., Shao, M., Lu, S.H., Wu, L.L., and Wang, X.M.: A gridded emission inventory of semi-volatile and intermediate volatility organic compounds in China. Sci. Total. Environ., 761, 143295, https://doi.org/10.1016/j.scitotenv.2020.143295, 2021b.

Wu, Y.J., Liu, P.J., Wang, Y.J., Wang, X.G., Zhang, J., Liu, Y., Zhang, J.S., Wu, L., Wang, T., Mao, H.J., and Peng, J.F.: Intermediate and semi-volatility organic compounds (I/SVOCs) emission from Chinese vehicles: volatility distribution, influencing factors, and implication for SOA formation. Front. Environ. Sci. Eng., 19: 70, https://doi.org/10.1007/s11783-025-1990-y, 2025a.

Wu, Y.J., Peng, J.F., Wang, X.G., Liu, P.J., Liu, Y., Zhang, F.Y., Zhang, J.S., Sun, B., Zhang, J.Q., Song, K., Song, P.F., Wu, L., Wang, T., Guo, S., and Mao, H.J.: Emissions and potential tracer screening of semivolatile/intermediate-volatility organic compounds from urban vehicle fleets. npj Clim Atmos Sci., 8, 186, https://doi.org/10.1038/s41612-025-01078-w, 2025b.

Yan, L., Zheng, B., Geng, G., Hong, C., Tong, D., and Zhang, Q.: Evaporation process dominates vehicular NMVOC emissions in China with enlarged contribution from 1990 to 2016. Environ. Res. Lett., 16, 124036, https://doi.org/10.1088/1748-9326/ac3872, 2021.

Yang, N., Wang, Q.Q., Xiong, Q., Fan, Z.M., Liu, G.J., Li, F., Zhu, S.W., Zhou, Y.Q., Tao, J.C., Hong, J., Wang, H.L., Huang, C., Sun, Y.L., Cheng, Y.F., Su, H., and Ma, N.: Intermediate-volatility organic compounds (IVOCs) emissions based on source-specific emission ratios relative to nonmethane volatile organic compounds (NMVOCs) give better representation of the spatial distribution of IVOCs in China. J. Geophys. Res.: Atmos., 130, e2024JD041464, https://doi.org/10.1029/2024JD041464, 2025.

Yang, W.Y., Li, J., Wang, W.G., Li, J.L., Ge, M.F., Sun, Y.L., Chen, X.S., Ge, B.Z., Tong, S.R., Wang, Q.Q., and Wang, Z.F.: Investigating secondary organic aerosol formation pathways in China during 2014. Atmos. Environ., 213, 133–147, https://doi.org/10.1016/j.atmosenv.2019.05.057, 2019.

Yang, X.P., Song, K., Guo, S., Wang, Y.J., Wang, J.F., Peng, D., Wen, Y., Li, A., Fan, B.M., Lu, S.H., and Ding, Y.: Elucidating the unexpected importance of intermediate-volatility organic compounds (IVOCs) from refueling procedure. J. Hazard. Mater., 471, 134361, https://doi.org/10.1016/j.jhazmat.2024.134361, 2024.

Zhang, J.S., Peng, J.F., Song, A.N., Du, Z.F., Guo, J.L., Liu, Y., Yang, Y.C., Wu, L., Wang, T., Song, K., Guo, S., Collins, D., and Mao, H.J.: Secondary organic aerosol formation

potential from vehicular non-tailpipe emissions under real-world driving conditions. Environ. Sci. Technol., 58, 5419–5429, https://doi.org/10.1021/acs.est.3c06475, 2024.

Zhang, Y.L., Wang, X.M., Zhang, Z., Lv, S.J., Shao, M., Lee, F.S.C., and Yu, J.Z.: Species profiles and normalized reactivity of volatile organic compounds from gasoline evaporation in China. Atmos. Environ., 79, 110–118, https://doi.org/10.1016/j.atmosenv.2013.06.029, 2013.

Zhao, B., Wang, S.X., and Hao, J.M.: Challenges and perspectives of air pollution control in China. Front. Environ. Sci. Eng., 18, 68, https://doi.org/10.1007/s11783-024-1828-z, 2024b.

Zhao, J.C., Lv, Z.F., Qi, L.J., Zhao, B., Deng, F.Y., Chang, X., Wang, X.T., Luo, Z.Y., Zhang, Z.N., Xu, H.L., Ying, Q., Wang, S.X., He, K.B., and Liu, H.: Comprehensive assessment for the impacts of S/IVOC emissions from mobile sources on SOA formation in China. Environ. Sci. Technol., 56, 16695–16706, https://doi.org/10.1021/acs.est.2c07265, 2022.

Zhao, S.Z., Jones, K.C., Weber, R., Xiao, Y.W., and Zhang, G.: Overlooked highly volatile persistent organic pollutants in the atmosphere. Environ. Sci. Technol., 58, 14062–14064, https://doi.org/10.1021/acs.est.4c02731, 2024a.

Zhao, Y.L., Hennigan, C., May, A.A., Tkacik, D., de Gouw, J. A., Gilman, J.B., Kuster, W.C., Borbon, A., and Robinson, A.L.: Intermediate-volatility organic compounds: a large source of secondary organic aerosol. Environ. Sci. Technol., 48, 13743–13750, https://doi.org/10.1021/es5035188, 2014.

Zhao, Y.L., Lambe, A.T., Saleh, R., Saliba, G., and Robinson, A.L.: Secondary organic aerosol production from gasoline vehicle exhaust: effects of engine technology, cold start, and emission certification standard. Environ. Sci. Technol., 52, 1253−1261, https://doi.org/10.1021/acs.est.7b05045, 2018.

Zhao, Y.L., Nguyen, N., Presto, A.A., Hennigan, C.J., May, A.A., and Robinson, A.L.: Intermediate volatility organic compound emissions from on-road diesel vehicles: chemical composition, emission factors, and estimated secondary organic aerosol production. Environ. Sci. Technol., 49, 11516–11526, https://doi.org/10.1021/acs.est.5b02841, 2015.

Zhao, Y.L., Nguyen, N.T., Presto, A.A., Hennigan, C.J., May. A.A., and Robinson, A.L.: Intermediate volatility organic compound emissions from on-road gasoline vehicles and small off-road gasoline engines. Environ. Sci. Technol., 50, 4554–4563, https://doi.org/10.1021/acs.est.5b06247, 2016.

Zheng, H.T., Chang, X., Wang, S.X., Li, S.Y., Yin, D.J., Zhao, B., Huang, G.H., Huang, L.Y., Jiang, Y.Q., Dong, Z.X., He, Y.C., Huang, C., and Xing, J.: Trends of full-volatility organic emissions in China from 2005 to 2019 and their organic aerosol formation

potentials. Environ. Sci. Technol. Lett., 10, 137–144, https://doi.org/10.1021/acs.estlett.2c00944, 2023.

Zheng, H.T., Wu, D., Wang, S.X., Li, X.D., Jin, L.N., Zhao, B., Li, S.Y., Sun, Y.S., Dong, Z. X., Wu, Q.R., Chen, X., Liu, Y.Z., Chen, J.M., Tian, H.Z., Liu, Q., Jiang, J.K., Kan, H.D., He, K.B., He, H., Chen, C.C., Zhao, J.C., Weichenthal, S., Ji, J.S., Cohen, A.J., Hao, J.M., and Li, Q.: Control of toxicity of fine particulate matter emissions in China. Nature, 643 (8071), 404–411, https://doi.org/10.1038/s41586-025-09158-w, 2025.

Zhou, Z.Y., Wang, Z.S., Feng, W., Qin, C., Liao, H., Wang, Y.H., and Xie, M.J.: Simulation of gas-particle partitioning of semi-volatile n-alkanes and PAHs in Nanjing, China, and Denver, United States: effects of vapor pressure and surface adsorption estimation. J. Geophys. Res. Atmos., 129, e2024JD041368, https://doi.org/10.1029/2024JD041368, 2024.

Zhu, Y.F., Liu, H., Cheng, H.X., Xi, Z.Q., Liu, X.F., and Xu, X.B.: The distribution and source apportionment of aliphatic hydrocarbons in soils from the outskirts of Beijing. Org. Geochem., 36, 475–483, https://doi.org/10.1016/j.orggeochem.2004.10.002, 2005.